Article

Analysis of Precise Orbit Determination of BDS-3 MEO and IGSO Satellites Based on Several Dual-Frequency Measurement Combinations

Bingfeng Tan , **Qingsong Ai *** **and Yunbin Yuan**

Innovation Academy for Precision Measurement Science and Technology, Chinese Academy of Sciences, West No.30 Xiao Hong Shan, Wuhan 430071, China
* Correspondence: aiqingsong@apm.ac.cn

Abstract: The Chinese BeiDou-3 navigation satellite system (BDS-3) is capable of transmitting both old B1I, B3I signals and new B1C, B2a, B2b signals. Current BDS-3 precise orbits are generally calculated using a B1I/B3I combination considering overlap with the BeiDou-2 navigation satellite system (BDS-2). In this contribution, the observation quality of BDS-3 medium earth orbit (MEO) satellites and inclined geosynchronous orbit (IGSO) satellites are analyzed based on three aspects, i.e., carrier to noise ratio (C/N0), pseudo-range noise and pseudo-range multipath (MP). The C/N0 of the MEO satellite is 2~3 dB higher than that of the IGSO satellite at the same elevation angle. Meanwhile, the order of the Root Mean Square (RMS) values of both pseudo-range noise and MP is B1I < B1C < B3I < B2a ≈ B2b. Three kinds of combinations, i.e., B1CB2a, B1CB2b and B1IB3I, are selected for the BDS-3 precise orbit determination (POD) experiment. Orbits are assessed by the orbit-only signal-in-space range error (SISRE) computed between pairs of the three kinds of combinations in this contribution, CODE and GFZ final orbits. Orbit-only SISRE assessment shows that B1CB2a/CODE, B1CB2b/CODE, B1CB2a/GFZ and B1CB2b/GFZ are at the same level with CODE/GFZ, and the orbit-only SISRE is at the level of 5 cm for MEOs and 9 cm for IGSOs, respectively. Meanwhile, B1IB3I/CODE and B1IB3I/GFZ are about 1–2 cm worse. Inter-solution comparison between B1CB2a, B1CB2b and B1IB3I also indicate that B1CB2a and B1CB2b have good consistency, while B1IB3I shows poor performance. Satellite laser ranging (SLR) residuals indicate that the mean RMS is 3–4 cm for the four BDS-3 MEOs for CODE final orbit, GFZ final orbit, B1CB2a and B1CB2b combinations, while the mean RMS value for B1IB3I combination is a few millimeters worse, at approximately 4–5 cm.

Keywords: precise orbit determination; BDS-3; carrier to noise ratio (C/N0); pseudo-range noise; pseudo-range multipath (MP); satellite laser ranging

1. Introduction

BDS-3 has been providing global services since Mid-2020 [1–3]. The operational status of the BDS-3 constellation is summarized in Table 1, as of October 2022. In addition to old B1I and B3I signals, BDS-3 satellites have been transmitting newly designed B1C, B2a and B2b signals [4], which are interoperable and compatible with the L1C/L5 frequencies of the global positioning system (GPS) and E1/E5 frequencies of European Galileo Navigation Satellite System (Galileo). These multi-frequencies bring forward the prospect for improving the performance of BDS3 POD. Yan et al. [5] demonstrated that the BDS-3 B1C signal has a lower C/N0 than B2a signal, which presents the same level compared with B1I or B3I signal. Zhang et al. [6] analyzed and reported that the observation noises of B1C and B2a are better than B1I. Based on nine Multi-GNSS pilot projects (MGEX) of the International GNSS Service (IGS), Li et al. [7] demonstrated that the POD result of BDS-3 satellites (C19-C37) in the B1C/B2a combination is preferable to the B1I/B3I combination.

Table 1. Operational status of the BDS-3 constellation as of October 2022.

Satellite	PRN	SVN	Type	Manufacture	Launch Date
BDS3-M01	C19	C201	MEO	CAST	5 November 2017
BDS3-M02	C20	C202	MEO	CAST	5 November 2017
BDS3-M03	C27	C203	MEO	SECM	1 January 2018
BDS3-M04	C28	C204	MEO	SECM	11 January 2018
BDS3-M05	C22	C205	MEO	CAST	12 February 2018
BDS3-M06	C21	C206	MEO	CAST	12 February 2018
BDS3-M07	C29	C207	MEO	SECM	29 March 2018
BDS3-M08	C30	C208	MEO	SECM	29 March 2018
BDS3-M09	C23	C209	MEO	CAST	29 July 2018
BDS3-M10	C24	C210	MEO	CAST	29 July 2018
BDS3-M11	C26	C211	MEO	SECM	24 August 2018
BDS3-M12	C25	C212	MEO	SECM	24 August 2018
BDS3-M13	C32	C213	MEO	CAST	19 September 2018
BDS3-M14	C33	C214	MEO	CAST	19 September 2018
BDS3-M15	C34	C215	MEO	SECM	15 October 2018
BDS3-M16	C35	C216	MEO	SECM	15 October 2018
BDS3-M17	C36	C218	MEO	CAST	18 November 2018
BDS3-M18	C37	C219	MEO	CAST	18 November 2018
BDS3-M19	C41	C227	MEO	CAST	16 December 2019
BDS3-M20	C42	C228	MEO	CAST	16 December 2019
BDS3-M21	C43	C226	MEO	SECM	23 November 2019
BDS3-M22	C44	C225	MEO	SECM	23 November 2019
BDS3-M23	C45	C222	MEO	CAST	22 September 2019
BDS3-M24	C46	C223	MEO	CAST	22 September 2019
BDS3-I01	C38	C220	IGSO	CAST	20 April 2019
BDS3-I02	C39	C221	IGSO	CAST	24 June 2019
BDS3-I03	C40	C224	IGSO	CAST	4 November 2019
BDS3-G01	C59	C217	GEO	CAST	1 November 2018
BDS3-G02	C60	C229	GEO	CAST	9 March 2020
BDS3-G03	C61	C230	GEO	CAST	2 June 2020

CAST: China Academy of Space Technology. SECM: Shanghai Engineering Center for Microsatellites, Chinese Academy of Sciences.

High-accuracy satellite orbit is the core technology for the operation and application of BDS. During the construction of BDS-2, analysis centers (ACs) of the International GNSS Monitoring and Assessment System (iGMAS), Center for Orbit Determination in Europe (CODE), Deutsches GeoForschungsZentrum (GFZ) and Technical University of Munich (TUM) have carried out much detailed research on POD of BDS-2. Montenbruck et al. [8] reported that the SLR residuals of the MGEX BDS-2 orbits were 5, 10 and 50 cm for MEOs, IGSOs, and GEOs, respectively. For BeiDou-3 experimental (BDS-3e) satellites, Tan et al. [9] reported the POD results of BDS-3e and BDS-2 based on 9 iGMAS stations, and SLR residuals demonstrated that the orbit radial component were 10 cm and 40 cm for the BDS-3e IGSO and MEO satellites, respectively. For BDS-3 satellites, based on 100 MGEX and iGMAS stations, Xu et al. [10] demonstrated that the SLR residual of the BDS-3 orbits was 4–6 cm. Meanwhile, several authors [11–15] have studied the BDS-3 POD based on inter-satellite links (ISLs), but ISL data are not used in the orbit product generation due to insufficient data openness.

As the inheritor of the multi-GNSS experiment established by the IGS, the MGEX has established a global observation network capable of collecting multi-GNSS signals. Currently, five MGEX ACs, i.e., CODE, Shanghai Astronomical Observatory (SHAO, CAS), GFZ, Information and Analysis Center (IAC) and Wuhan University (WHU) have been offering multi-GNSS orbits with BDS-3 included [16–20]. Steigenberger et al. [21] have conducted an orbit consistency analysis and SLR analysis of the five MGEX Acs. It should be noticed that the B1I/B3I combination is widely used in the BDS-3 product solution among these ACs, in consideration of the overlap with BDS-2 [22–24].

Due to the limited amount of tracking stations supporting the BDS-3 new B1C, B2a and B2b signals, and consideration for the compatibility with BDS-2, current BDS-3 POD research work and orbit products are restricted to the old B1I/B3I combination. There is little research on POD of the BDS-3 constellation based on different dual-frequency measurement combinations, especially B2b signal [25–28], and there is still limited research on observation quality analysis of BDS-3 new signals, especially the B2b signal [29–31]. We need to investigate the observation quality of BDS-3 operational signals, i.e., B1C, B2a, B2b, B1I and B3I. We should also analyze the BDS-3 satellite POD performance based on new B1C, B2a and B2b combinations by comparing with the old B1IB3I combination. In this contribution, POD of BDS-3 satellites based on several dual-frequency measurement combinations are presented.

The algorithm for observation quality analysis with C/N0, pseudo-range noise and pseudo-range MP, the MGEX tracking stations used to estimate the BDS-3 orbits and the POD procedure are shown in Section 2. Meanwhile, orbits are validated by the orbit-only SISRE computed between B1CB2a combination, B1CB2b combination, B1IB3I combination, CODE and GFZ final orbits. Moreover, SLR validation is conducted. The corresponding results are shown and investigated in Section 3. Finally, some key aspects are further discussed and a conclusion is formed in the last Section.

2. Methods

2.1. MGEX Tracking Network

As of the middle of 2022, the MGEX tracking network contains about 520 stations, more than 300 of them are capable of tracking BDS. However, not of all these stations are applicable for BDS satellite POD, mainly due to deficiency of frequencies or pseudo-random noise (PRN) number supporting capability. Based on the statistics of multi-GNSS observations during July 2022 from the Crustal Dynamics Data Information System (CDDIS) [32], 129 MGEX stations with the capability of tracking all BDS-3 B1I, B3I, B1C, B2a and B2b signals are recognized and selected for the BDS-3 satellite POD experiment, and Figure 1 demonstrates the station distribution. One month observations from 1 July 2022 to 31 July 2022 are selected for the POD experiment.
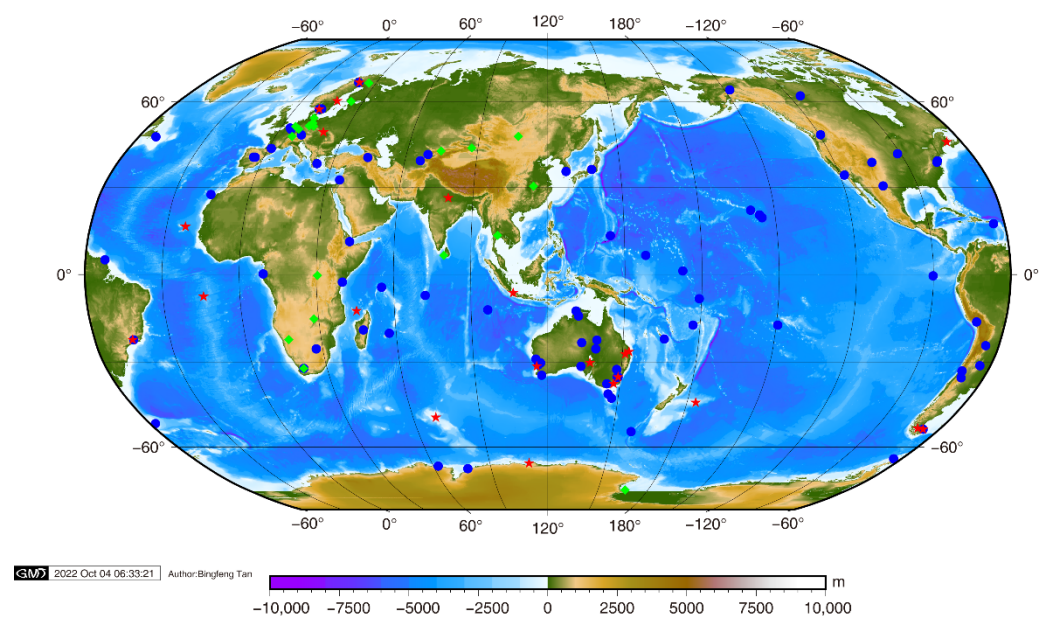
Figure 1. Tracking stations selected for BDS-3 POD. Sites are marked by green diamonds, blue circles and red five-pointed stars for Javad receivers, Septentrio receivers and Trimble receivers, respectively.

2.2. Tracking Data Analysis Algorithm

The quality of observations is the footstone of BDS-3 POD. The following is a brief description of some indices commonly used in tracking data quality analysis.

(1) C/N0 analysis

C/N0 is mainly affected by parameters of antenna gain, multipath and the condition of correlator in receiver. It is an index reflecting the quality of carrier phase observations. C/N0 can be obtained through the observations [33–37].

(2) Pseudo-range MP analysis

When the GNSS observation signal is received by a station, it will generate a variety of reflected signals due to the interference of the surrounding environment, making the received signal deviate from true value, which is called MP. Compared with pseudo-range MP, carrier phase MP is negligible. The pseudo-range MP can be expressed as:

$$MP_i = P_i - \lambda_i \varphi_i - \frac{2 f_i^2}{f_i^2 - f_j^2} \left(\lambda_i \varphi_i - \lambda_j \varphi_j \right) - B_i \tag{1}$$

where i and j are frequency band with the value, $i, j = 1, 2, 3 \ldots (i \neq j)$, P_i and φ_i are the observations of pseudo-range and carrier phase, λ_i is the wavelength of frequency, B_i contains the linear combination of the phase ambiguities and the constant part of the hardware delays which can be obtained with the mean value within a continuous observation arc [38].

(3) Pseudo-range noise analysis

The pseudo-range noise can be expressed with difference between pseudo-range and carrier phase observations (code minus carrier phase, *CC*). Considering the high accuracy of carrier phase observations, the phase multipath is negligible, then *CC* can be expressed as follows.

$$CC_i = P_i - \lambda_i \varphi_i \tag{2}$$

2.3. POD Strategy of BDS-3 Satellite Based on Several Dual-Frequency Measurement Combinations

Important aspects and detailed description regarding GFZ solution, CODE solution, B1CB2a, B1CB2b and B1IB3I combinations in this contribution are summarized in Table 2.

Table 2. BDS-3 satellite POD strategy and important aspects for GFZ solution, CODE solution and B1CB2a, B1CB2b and B1IB3I combinations.

|	**GFZ Solution**	**CODE Solution**	**B1CB2a, B1CB2b and B1IB3I Combinations**
Platform	EPOS	Bernese GNSS Software version 5.3	Modified Bernese GNSS Software version 5.2
Stations used for satellite POD	160 stations	140 stations, with 90 stations supporting BDS-3	129 stations, all supporting BDS-3
Signals used for BDS-3 POD	B1IB3I	B1IB3I	B1CB2a, B1CB2b and B1IB3I
Data differencing strategy	Undifferenced	Double differenced	Double differenced
Data coverage	24 h arc	72 h arc	72 h arc
Sampling rate	300 s	180 s	180 s
Elevation angle cut-off	7°	3°	3°
Weighting	Elevation-dependent weighting	Elevation-dependent weighting	Elevation-dependent weighting, and 6 mm threshold value for carrier phase residuals
A prior orbits	Rapid products	Rapid products	Based on broadcast ephemeris

Table 2. *Cont.*

	GFZ Solution	CODE Solution	B1CB2a, B1CB2b and B1IB3I Combinations
Satellite and receiver antenna PCO/PCV	igs14.atx for both satellite and receiver antennas	CSNO value for satellite antennas, and igsR3.atx for receiver antennas	igs14_2218.atx for satellite antennas. For receiver antennas, GPS L1/L2 values adopted for all dual-frequency measurement combinations of BDS-3 [39]
Antenna thrust for CAST MEO, SECM MEO and CAST IGSO	310 W/280 W/100 W	310 W/280 W/0 W	Not applied
Earth albedo	Not applied	Not applied	Not applied
Troposphere	1 h random-walk for zenith delay and 2 h random-walk for gradients	2 h piece-wise linear for zenith delay and 24 h piece-wise linear for gradients	2 h piece-wise linear for zenith delay and 24 h piece-wise linear for gradients
Ambiguities	Fixed	Fixed	Fixed
Pseudo-stochastic orbit parameters	At noon in radial, along-track and cross-track direction	12 h in radial, along-track and cross-track direction	Every 12 h, with the constraint of 1×10^{-6} m/s, 1×10^{-5} m/s and 1×10^{-8} m/s in the radial, along-track and cross-track direction, respectively
Precession and nutation	IAU 2000	IAU 2000 and IAU 2000R06	IAU 2000
Geopotential	EGM2008	EGM2008 12×12	EGM2008 12×12
Solid Earth tides, ocean tides and solid Earth pole tides	IERS Conventions 2010	IERS Conventions 2010	IERS Conventions 2010 [40]
N body gravitation	DE421 ephemeris from JPL	DE421 ephemeris from JPL	DE405 ephemeris from JPL
A prior Solar Radiation Pressure (SRP) model	None	None	None
SRP model	Empirical CODE Orbit Model, ECOM (D0, Y0, B0, BC, BS)	The new extended ECOM, ECOM-2 (D0, Y0, B0, BC, BS, D2C, D2S)	The new extended ECOM, ECOM-2 (D0, Y0, B0, BC, BS, D2C, D2S) [41]

The Bernese GNSS Software version 5.2, developed by CODE, has been updated to support BDS-3 POD in this contribution. Similar to Galileo MEOs which hold a rectangular shape, ECOM is not capable of appropriately modeling the solar radiation pressure for BDS-3 satellites. Hence, the same as CODE AC, ECOM-2 is used in this contribution.

Five signals of BDS-3 have been chosen, and three types of dual-frequency measurement combinations, i.e., B1CB2a, B1CB2b and B1IB3I are employed in BDS-3 POD processing. It should be emphasized that, except for the different signals used, other strategies are the same for BDS-3 POD based on B1CB2a, B1CB2b and B1IB3I combinations in this contribution. The BDS-3 POD procedure based on B1CB2a, B1CB2b and B1IB3I combinations are summarized in Figure 2. For GFZ and CODE final orbits, only B1IB3I combination is used, considering the compatibility with BDS-2.
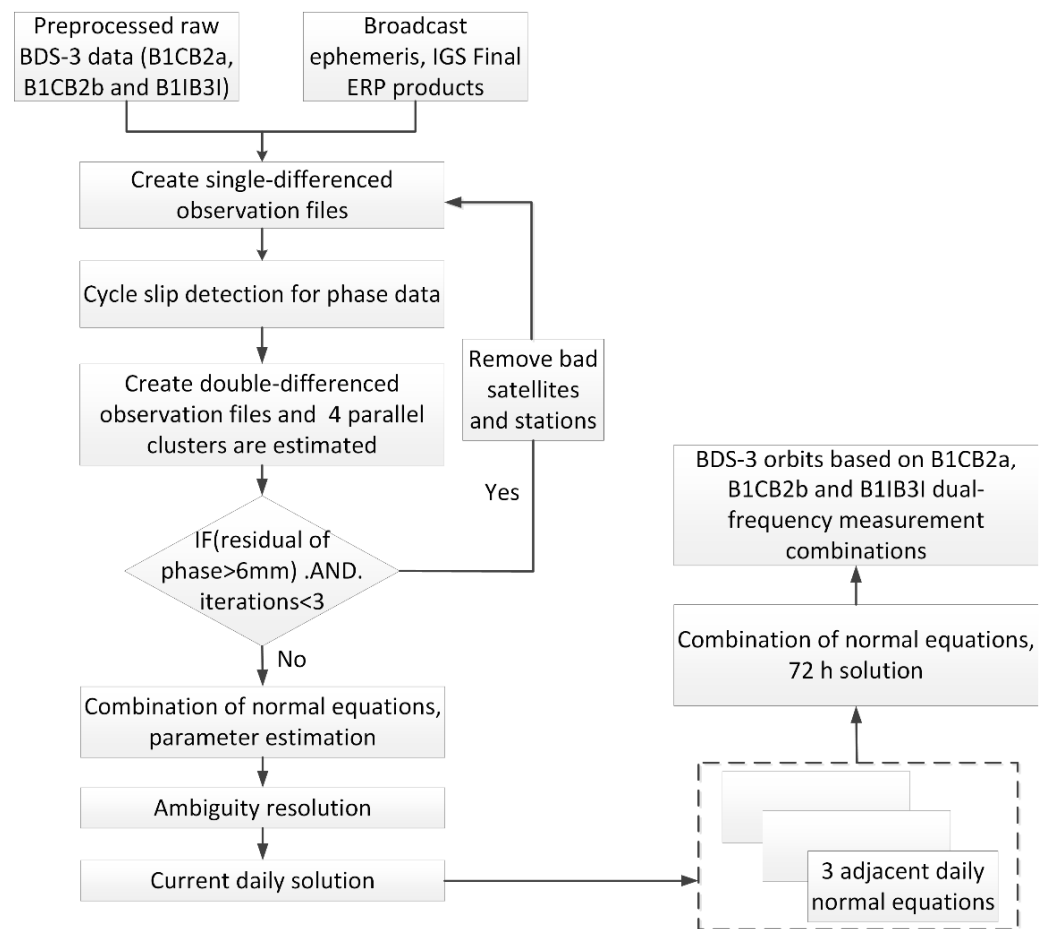
Figure 2. Flowchart of BDS-3 POD procedure based on B1CB2a, B1CB2b and B1IB3I dual-frequency measurement combinations.

3. Results

3.1. Tracking Data Analysis

Considering the periodicity of POD, a week's (25 July 2022 to 31 July 2022) MGEX tracking data are adopted for analysis. A typical representative of BDS-3 MEOs (C21, C23, C29) and IGSOs (C38, C39, C40) detail tracking data analysis are displayed in Figures 3–6 and all the BDS-3 satellite statistical information is listed in Table 3.
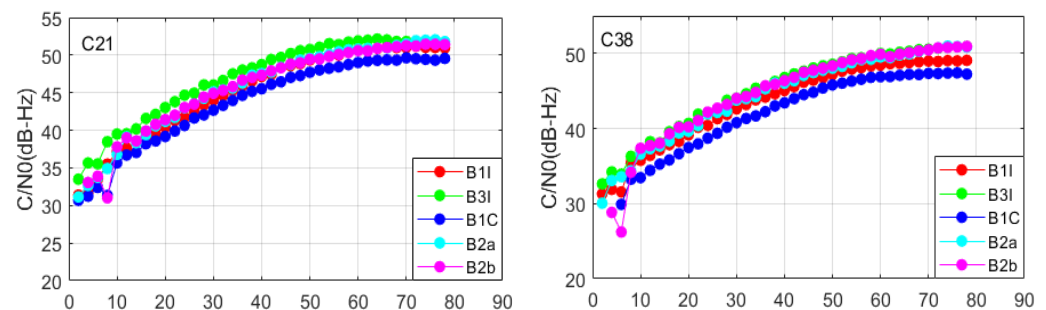
Figure 3. *Cont*.
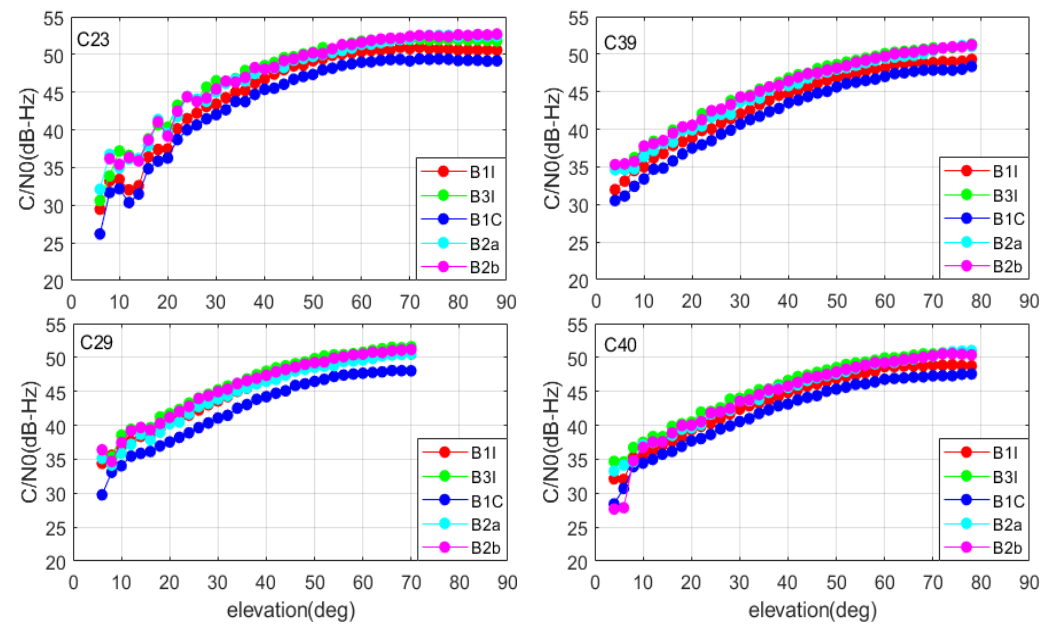
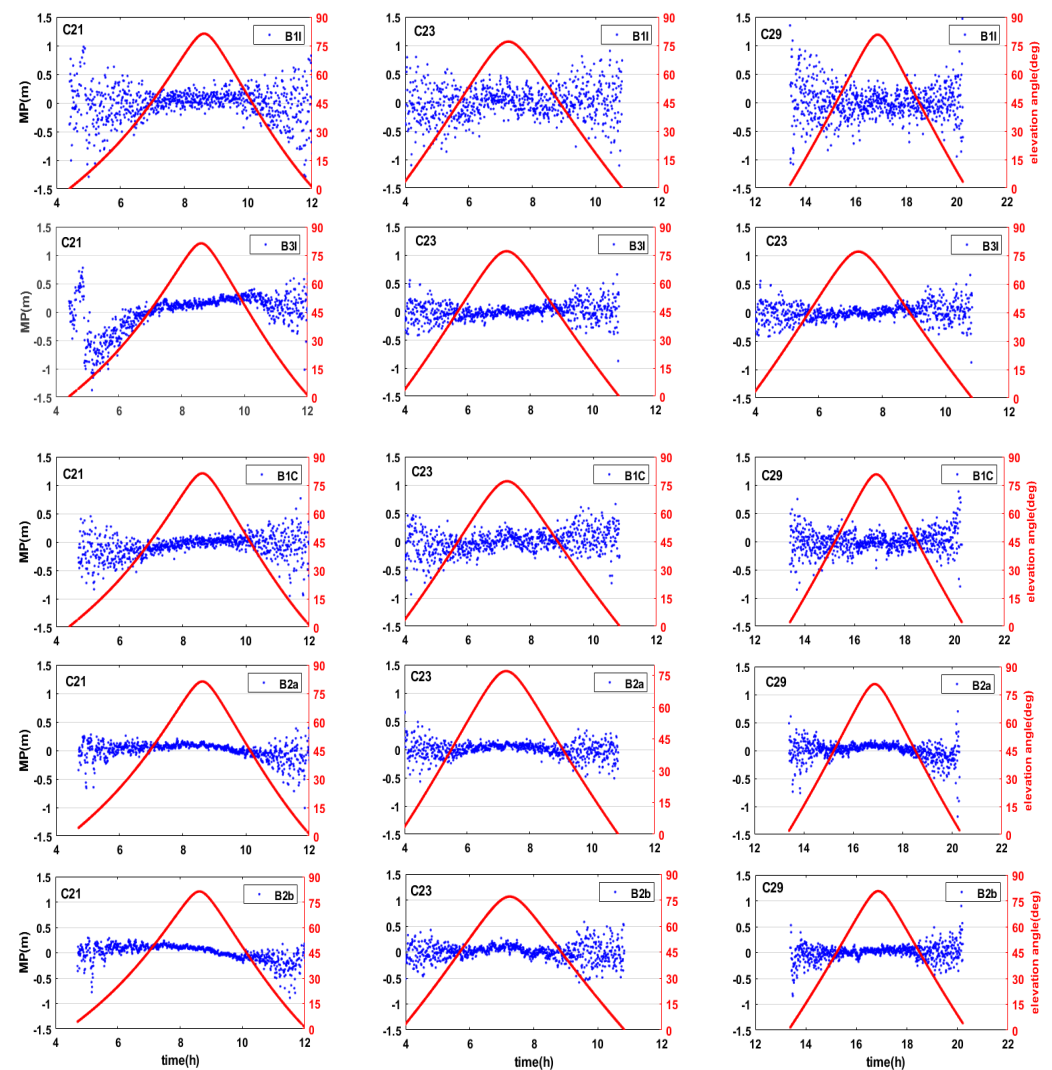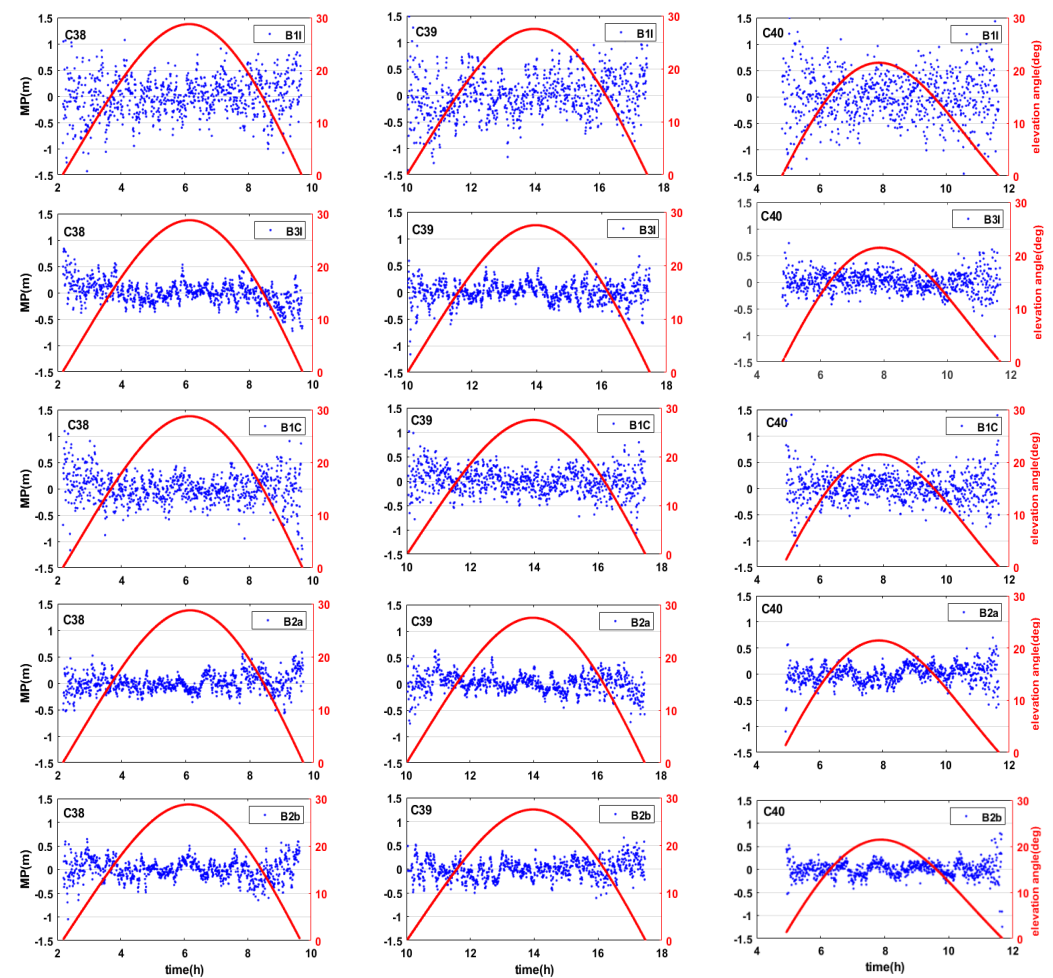**Figure 3.** Average C/N0 series of BDS-3 satellites in different frequency.

Figure 4. The MP series of BDS-3 MEO satellites in different frequencies.

Figure 5. The MP series of BDS-3 IGSO satellites in different frequencies.

(1) C/N0 analysis

As in Figure 3, the C/N0 of each frequency varies at the same level of 30 dB to 55 dB, and the C/N0 tends to be stable when the elevation angle reaches 60 degrees. The C/N0 of MEO satellite is 2~3 dB larger than that of IGSO at the same elevation angle. This may be caused by the higher orbital height and the lower satellite transmission power of the IGSO satellite. The correlation trend of C/N0 between each frequency point and the elevation angle is almost the same. Both the C/N0 of MEO and IGSO has the same sort of B3I > B2b > B2a > B1I > B1C.

(2) Pseudo-range MP analysis

As in Figures 4 and 5 and Table 3, the MP of the MEO satellite has systematic variation at each frequency. With the increase in elevation angle, the MP becomes smaller, and it tends to be stable while the elevation angle is greater than 50 deg. The MP of IGSOs shows no obvious systematic variation with elevation angle. The average MP of MEOs is obviously smaller than that of IGSOs, which may be due to the large number of low elevation angles during the IGSO satellite observation period. In general, the MP trend of MEOs and IGSOs have the same sort of B1I > B1C > B3I > B2a ≈ B2b, and all the MPs fluctuate within ±0.5 m.

(3) Pseudo-range noise analysis

As in Figure 6 and Table 3, the pseudo-range noise of B1C is much larger than that of B2a. Based on the statistical results, it can also be discovered that the noise of B1C is 0.3 m and 0.24 m for IGSOs and MEOs, which is larger than that of a B2a signal with 0.21 m and

0.18 m for IGSOs and MEOs, respectively. The pseudo-range noise of B3I is significantly better than B1I, and the noise of these two signals are in the range of 0.2~0.4 m. Meanwhile, the noise of B3I and B1I is slightly worse than B2a, while the noise of B2a is almost equal to B2b which is in the range of 0.18~0.22 m. For BDS-3, the pseudo-range noise accuracies of MEOs are better than those of IGSOs, which may be because IGSOs have a large proportion of low elevation angle observation periods, resulting in more pseudo-range noise. Overall, pseudo-range measurement accuracy is in the following order: B2b ≈ B2a > B3I > B1C > B1I.
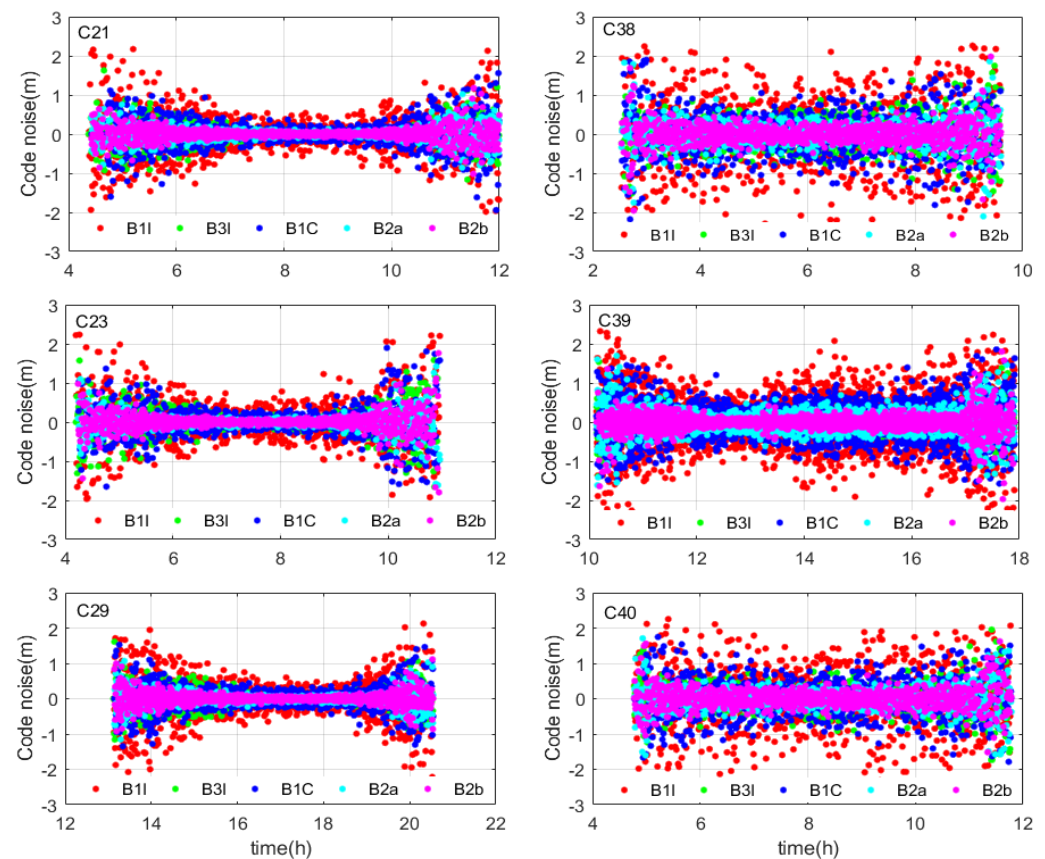
Figure 6. The pseudo-range noise series of BDS-3 satellites in different frequencies.

Table 3. RMS statistics of observation quality for BDS-3 IGSOs and MEOs.

Type/Frequency	IGSOs			MEOs		
	C/N0 (dB-Hz)	MP (m)	Pseudo-Range Noise (m)	C/N0 (dB-Hz)	MP (m)	Pseudo-Range Noise (m)
B1I	45.18	0.48	0.40	47.28	0.40	0.33
B3I	47.23	0.29	0.23	48.78	0.23	0.20
B1C	43.88	0.32	0.30	45.84	0.26	0.24
B2a	45.27	0.26	0.21	47.49	0.23	0.18
B2b	45.93	0.24	0.22	47.97	0.22	0.18

3.2. Orbit Quality

The SISRE [42,43] is widely adopted for the quality validation of satellite ephemerides and can also be adapted to assess the consistency of orbit and clock products from different agencies with similar precision. In this contribution, the SISRE computed between B1CB2a combination, B1CB2b combination, B1IB3I combination, CODE and GFZ final orbits are used for orbit precision validation. Meanwhile, SLR validation is used for orbit accuracy assessment. The POD assessment spans from 1 July 2022 to 31 July 2022.
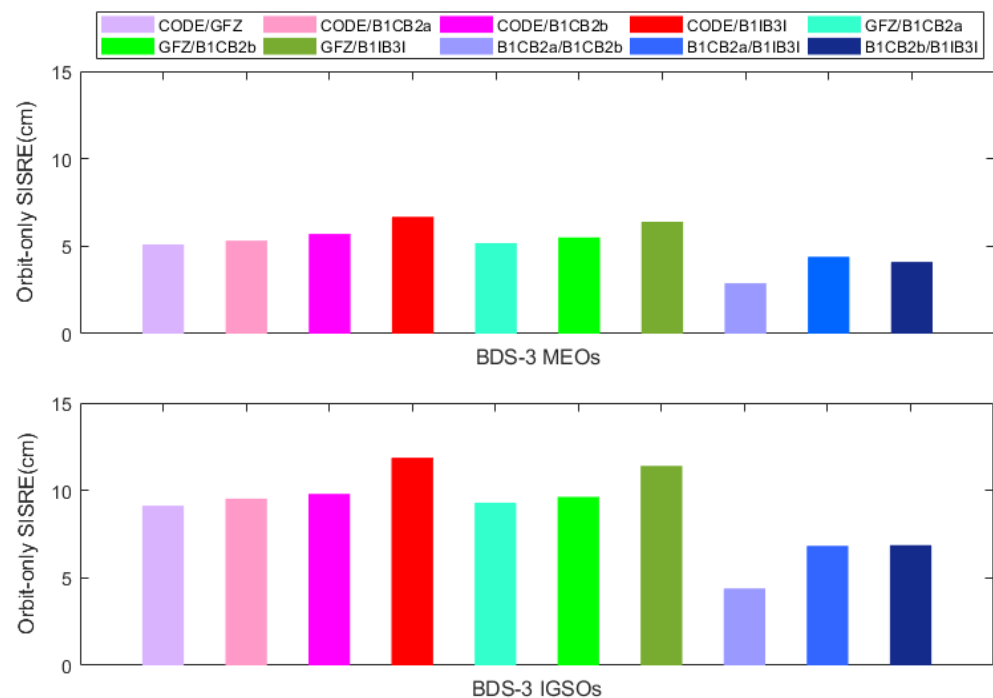
3.2.1. Orbit-Only SISRE

The orbit and clock SISRE are obtained as follows:

$$SISRE = \sqrt{\left(w_1^2 R^2 - 2w_1 RT + T^2\right) + w_2^2(A^2 + C^2)} \tag{3}$$

where *R*, *A* and *C* represent the satellite orbit difference in radial, along-track and cross-track directions, respectively. *T* denotes the satellite clock difference, and orbit-only SISRE can be obtained by setting *T* to zero. Meanwhile, Montenbruck et al. [42] published the recommended value of w_1 and w_2 in Table 4 of the paper, and the value is adopted in this contribution for our orbit-only SISRE investigation. Table 4 and Figure 7 illuminate the orbit-only SISRE for BDS-3 MEOs and IGSOs computed between B1CB2a combination, B1CB2b combination, B1IB3I combination, CODE and GFZ final orbits.

Table 4. Orbit-only SISRE for MEOs and IGSOs of BDS-3 between different solutions.

Combination1/AC1	Combination2/AC2	Orbit-Only SISRE (cm)	
		MEOs	**IGSOs**
CODE	GFZ	5.10	9.13
CODE	B1CB2a	5.32	9.53
CODE	B1CB2b	5.70	9.80
CODE	B1IB3I	6.68	11.87
GFZ	B1CB2a	5.18	9.30
GFZ	B1CB2b	5.50	9.63
GFZ	B1IB3I	6.40	11.40
B1CB2a	B1CB2b	2.88	4.40
B1CB2a	B1IB3I	4.40	6.83
B1CB2b	B1IB3I	4.10	6.87

Figure 7. Histogram of the orbit-only SISRE for MEOs and IGSOs of BDS-3 between different solutions.

In Figure 7, CODE/GFZ represents the orbit-only SISRE between CODE orbit and GFZ orbit. Meanwhile, CODE/B1CB2a, CODE/B1C2b and CODE/B1IB3I stand for the orbit-only SISRE between CODE orbit and dual-frequency measurement combinations in this contribution. Similarly, GFZ/B1CB2a, GFZ/B1C2b and GFZ/B1IB3I stand for the orbit-

only SISRE between GFZ orbit and dual-frequency measurement combinations. Finally, B1CB2a/B1CB2b, B1CB2a/B1IB3I and B1CB2b/B1IB3I symbolize internal orbit-only SISRE comparison results for the three dual-frequency measurement combinations.

For external consistency comparison with CODE and GFZ final orbits, B1CB2a/CODE, B1CB2b/CODE, B1CB2a/GFZ and B1CB2b/GFZ are at the same level as CODE/GFZ, the orbit-only SISRE approximately 5 cm for MEOs and 9 cm for IGSOs, respectively. Meanwhile, B1IB3I/CODE and B1IB3I/GFZ are about 1–2 cm worse for both MEOs and IGSOs, at approximately 6 cm for MEOs and 11 cm for IGSOs, respectively. For internal coincidence comparison, the consistency of B1CB2a/B1CB2b is also superior to that of the B1CB2a/B1IB3I and B1CB2b/B1IB3I combinations. Moreover, the orbit-only SISRE for IGSOs is significantly larger than that of the MEOs, mainly due to the ground tracking station coverage for these IGSOs and SRP modelling difficulties caused by large communication antennas.
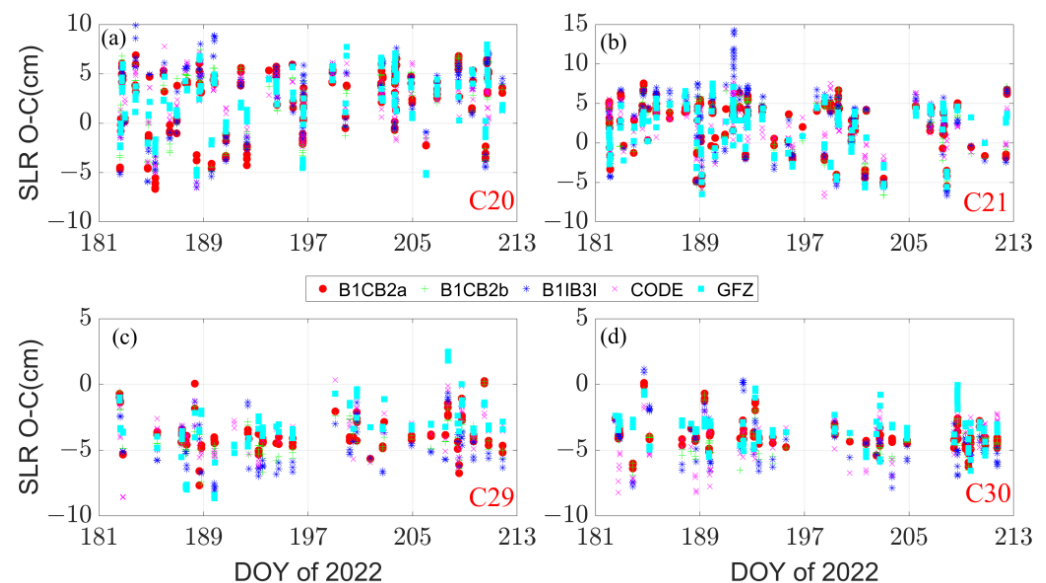
3.2.2. SLR Residuals

To further investigate the orbit accuracy of BDS-3 POD solutions, SLR tracking data has been used to assess the orbits. Two BDS-3 MEOs (C20/M2, C21/M3) manufactured by CAST and two BDS-3 MEOs (C29/M9, C30/M10) manufactured by SECM are regularly observed by the International Laser Ranging Service (ILRS) [44]. The system eccentricities and station coordinates are updated and fixed to SLRF2014, and the retro-reflector offsets of the MEOs are given by CSNO [45]. SLR observations from 1 July 2022 to 31 July 2022 collected by ILRS have been processed. The statistics of the SLR validation is demonstrated in Table 5 and shown in Figure 8.

Table 5. Mean value and mean RMS of SLR residuals of BDS-3 MEOs.

PRN of BDS-3	Solutions	Mean Value (cm)	Mean RMS (cm)
	CODE	2.24	3.50
	GFZ	2.55	3.90
C20, M2 (CAST)	B1CB2a	2.34	4.13
	B1CB2b	2.54	4.20
	B1IB3I	2.94	4.83
	CODE	2.27	3.58
	GFZ	1.82	3.54
C21, M3 (CAST)	B1CB2a	2.44	4.02
	B1CB2b	2.47	4.12
	B1IB3I	3.01	5.25
	CODE	−3.68	4.03
	GFZ	−3.19	3.87
C29, M9 (SECM)	B1CB2a	−3.74	4.01
	B1CB2b	−4.07	4.35
	B1IB3I	−4.64	5.03
	CODE	−4.37	4.68
	GFZ	−3.36	3.61
C30, M10 (SECM)	B1CB2a	−3.89	4.05
	B1CB2b	−4.26	4.43
	B1IB3I	−4.48	4.86

The SLR validation results basically coincide with the orbit-only SISRE investigation. For CODE, GFZ, B1CB2a and B1CB2b solutions, the mean RMS of SLR residuals are 3–4 cm and the mean values are approximately 2 cm and −4 cm for CAST and SECM satellites, respectively. Meanwhile, the mean RMS of B1IB3I solution is a few millimeters worse, which is approximately 4–5 cm. Moreover, mean values of SLR residuals for BDS-3 CAST and SECM satellites point to remaining deficiencies in BDS-3 satellite empirical solar radiation pressure modelling.

Figure 8. SLR residuals of BDS-3 four MEOs for different solutions. (**a**) for M2/C20, (**b**) for M3/C21, (**c**) for M9/C29, and (**d**) for M10/C30, respectively.

4. Conclusions

In the literature, many studies expounded the BDS-3 POD based on B1I/B3I combination, and few works analyzed BDS-3 POD based on all of the new signals. In this contribution, the observation quality of BDS-3 MEOs and IGSOs is analyzed. This indicates that C/N0 of MEO satellite is 2~3 dB higher than that of IGSO satellite at the same elevation angle. Meanwhile, the pseudo-range MP and noise for all operational signals of BDS-3 satellites are better than IGSO due to the lower satellite transmission power and the low elevation angle observation period. The overall observation quality of BDS-3 MEOs and IGSOs in each frequency is B1I < B1C < B3I < B2a ≈ B2b.

One month of observations from 129 MGEX stations are processed for BDS-3 POD based on three different combinations, i.e., B1CB2a, B1CB2b and B1IB3I. The inter-agency consistency is assessed by orbit-only SISRE comparison between B1CB2a combination, B1CB2b combination, B1IB3I combination, CODE and GFZ final orbits. The B1CB2a and B1CB2b combinations are superior to the B1IB3I combination when compared with CODE or GFZ final orbits. Orbit-only SISRE for B1CB2a/CODE, B1CB2b/CODE, B1CB2a/GFZ, B1CB2b/GFZ and CODE/GFZ is approximately 5 cm for MEOs and 9 cm for IGSOs, respectively. Meanwhile, B1IB3I/CODE and B1IB3I/GFZ are about 1–2 cm worse. Comparison between B1CB2a, B1CB2b and B1IB3I also indicates that B1CB2a and B1CB2b have good consistency, while B1IB3I shows poor performance. Moreover, the performance of IGSOs is significantly worse than that of MEOs due to the geographical distribution of ground tracking stations and SRP modelling problems which should be further investigated. As for the orbit accuracy investigation by the SLR technique, result is in good agreement with the orbit-only SISRE assessment. For CODE orbit, GFZ orbit, B1CB2a and B1CB2b solutions, the mean RMS is 3–4 cm and the mean values are approximately 2 cm and −4 cm for CAST and SECM satellites, respectively. As for B1IB3I solution, the mean RMS value is a few millimeters worse, which is approximately 4–5 cm. Moreover, mean values of SLR residuals for BDS-3 CAST and SECM satellites also demonstrate that deficiencies still exist in BDS-3 satellite empirical SRP modelling, i.e., ECOM and ECOM-2.

In summary, the BDS-3 new signals such as B1C, B2a, and B2b are significantly better than the old B1I and B3I signals not only in observation quality but also in POD performance. We recommend using B1CB2a or B1CB2b combinations for BDS-3 POD, and BDS-2 can be handled as an individual constellation using the B1IB3I combination.

References

1. Yang, Y.; Gao, W.; Guo, S.; Mao, Y.; Yang, Y. Introduction to BeiDou-3 navigation satellite system. *Navigation* **2019**, *66*, 7–18. [CrossRef]
2. Yang, Y.; Mao, Y.; Sun, B. Basic performance and future developments of BeiDou global navigation satellite system. *Satell. Navig.* **2020**, *1*, 1. [CrossRef]
3. Yang, Y.; Xu, Y.; Li, J.; Yang, C. Progress and performance evaluation of BeiDou global navigation satellite system: Data analysis based on BDS-3 demonstration system. *Sci. China Earth Sci.* **2018**, *61*, 614–624. [CrossRef]
4. Lu, M.; Li, W.; Yao, Z.; Cui, X. Overview of BDS III new signals. *Navigation* **2019**, *66*, 19–35. [CrossRef]
5. Yan, X.; Huang, G.; Zhang, Q.; Liu, C.; Wang, L.; Qin, Z. Early analysis of precise orbit and clock offset determination for the satellites of the global BeiDou-3 system. *Adv. Space Res.* **2019**, *63*, 1270–1279. [CrossRef]
6. Zhang, B.; Jia, X.; Sun, F.; Xiao, K.; Dai, H. Performance of BeiDou-3 satellites: Signal quality analysis and precise orbit determination. *Adv. Space Res.* **2019**, *64*, 687–695. [CrossRef]
7. Li, R.; Wang, N.; Li, Z.; Zhang, Y.; Wang, Z.; Ma, H. Precise orbit determination of BDS-3 satellites using B1C and B2a dual-frequency measurements. *GPS Solut.* **2021**, *25*, 95. [CrossRef]
8. Montenbruck, O.; Steigenberger, P.; Prange, L.; Deng, Z.; Zhao, Q.; Perosanz, F.; Romero, I.; Noll, C.; Stürze, A.; Weber, G. The Multi-GNSS Experiment (MGEX) of the International GNSS Service (IGS)–achievements, prospects and challenges. *Adv. Space Res.* **2017**, *59*, 1671–1697. [CrossRef]
9. Tan, B.; Yuan, Y.; Wen, M.; Ning, Y.; Liu, X. Initial results of the precise orbit determination for the new-generation BeiDou satellites (BeiDou-3) based on the iGMAS network. *ISPRS Int. J. Geo-Inf.* **2016**, *5*, 196. [CrossRef]
10. Xu, X.; Wang, X.; Liu, J.; Zhao, Q. Characteristics of BD3 global service satellites: POD, open service signal and atomic clock performance. *Remote Sens.* **2019**, *11*, 1559. [CrossRef]
11. Cinelli, M.; Ortore, E.; Laneve, G.; Circi, C. Geometrical approach for an optimal inter-satellite visibility. *Astrodynamics* **2021**, *5*, 237–248. [CrossRef]
12. Kai, X.; Chunling, W.; Liangdong, L. Autonomous navigation for a group of satellites with star sensors and inter-satellite links. *Acta Astronaut.* **2013**, *86*, 10–23. [CrossRef]
13. Wang, C.; Zhao, Q.; Guo, J.; Liu, J.; Chen, G. The contribution of intersatellite links to BDS-3 orbit determination: Model refinement and comparisons. *Navigation* **2019**, *66*, 71–82. [CrossRef]
14. Xie, X.; Geng, T.; Zhao, Q.; Lv, Y.; Cai, H.; Liu, J. Orbit and clock analysis of BDS-3 satellites using inter-satellite link observations. *J. Geod.* **2020**, *94*, 64. [CrossRef]
15. Yu, F.; He, Z.; Xu, N. Autonomous navigation for GPS using inter-satellite ranging and relative direction measurements. *Acta Astronaut.* **2019**, *160*, 646–655. [CrossRef]
16. Deng, Z.; Nischan, T.; Bradke, M. *Multi-GNSS Rapid Orbit-, Clock- & EOP-Product Series*; GFZ Data Services: Potsdam, Germany, 2017.
17. Guo, J.; Xu, X.; Zhao, Q.; Liu, J. Precise orbit determination for quad-constellation satellites at Wuhan University: Strategy, result validation, and comparison. *J. Geod.* **2016**, *90*, 143–159. [CrossRef]
18. Prange, L.; Villiger, A.; Sidorov, D.; Schaer, S.; Beutler, G.; Dach, R.; Jäggi, A. Overview of CODE's MGEX solution with the focus on Galileo. *Adv. Space Res.* **2020**, *66*, 2786–2798. [CrossRef]
19. Zhao, Q.; Guo, J.; Wang, C.; Lyu, Y.; Xu, X.; Yang, C.; Li, J. Precise orbit determination for BDS satellites. *Satell. Navig.* **2022**, *3*, 2. [CrossRef]
20. Zhou, W.; Cai, H.; Chen, G.; Jiao, W.; He, Q.; Yang, Y. Multi-GNSS Combined Orbit and Clock Solutions at iGMAS. *Sensors* **2022**, *22*, 457. [CrossRef]

21. Steigenberger, P.; Deng, Z.; Guo, J.; Prange, L.; Song, S.; Montenbruck, O. BeiDou-3 orbit and clock quality of the IGS Multi-GNSS Pilot Project. *Adv. Space Res.* **2022**, *in press*. [CrossRef]

22. Xie, X.; Geng, T.; Zhao, Q.; Liu, J.; Wang, B. Performance of BDS-3: Measurement quality analysis, precise orbit and clock determination. *Sensors* **2017**, *17*, 1233. [CrossRef] [PubMed]

23. Zhang, X.; Wu, M.; Liu, W.; Li, X.; Yu, S.; Lu, C.; Wickert, J. Initial assessment of the COMPASS/BeiDou-3: New-generation navigation signals. *J. Geod.* **2017**, *91*, 1225–1240. [CrossRef]

24. Tan, B.; Yuan, Y.; Ai, Q.; Zha, J. Real-Time Multi-GNSS Precise Orbit Determination Based on the Hourly Updated Ultra-Rapid Orbit Prediction Method. *Remote Sens.* **2022**, *14*, 4412. [CrossRef]

25. Ai, Q.; Yuan, Y.; Zhang, B.; Xu, T.; Chen, Y. Refining GPS/GLONASS Satellite Clock Offset Estimation in the Presence of Pseudo-Range Inter-Channel Biases. *Remote Sens.* **2020**, *12*, 1821. [CrossRef]

26. Ai, Q.; Zhang, B.; Yuan, Y.; Xu, T.; Chen, Y.; Tan, B. Evaluation and mitigation of the influence of pseudorange biases on GNSS satellite clock offset estimation. *Measurement* **2022**, *193*, 111015. [CrossRef]

27. Cao, Y.; Huang, G.; Xie, W.; Xie, S.; Wang, H. Assessment and comparison of satellite clock offset between BeiDou-3 and other GNSSs. *Acta Geod. Geophys.* **2021**, *56*, 303–319. [CrossRef]

28. Li, X.; Hu, X.; Guo, R.; Tang, C.; Zhou, S.; Liu, S.; Chen, J. Orbit and positioning accuracy for new generation BeiDou satellites during the earth eclipsing period. *J. Navig.* **2018**, *71*, 1069–1087. [CrossRef]

29. Li, X.; Yuan, Y.; Zhu, Y.; Jiao, W.; Bian, L.; Li, X.; Zhang, K. Improving BDS-3 precise orbit determination for medium earth orbit satellites. *GPS Solut.* **2020**, *24*, 53. [CrossRef]

30. Lin, X.; Baojun, L.; Yingchun, L.; Sujie, X.; Tao, B. Satellite geometry and attitude mode of BDS-3 MEO satellites developed by SECM. In Proceedings of the 31st International Technical Meeting of the Satellite Division of the Institute of Navigation (ION GNSS+ 2018), Miami, FL, USA, 24–28 September 2018; pp. 1268–1289.

31. Wanninger, L.; Beer, S. BeiDou satellite-induced code pseudorange variations: Diagnosis and therapy. *GPS Solut.* **2015**, *19*, 639–648. [CrossRef]

32. Noll, C.E. The crustal dynamics data information system: A resource to support scientific analysis using space geodesy. *Adv. Space Res.* **2010**, *45*, 1421–1440. [CrossRef]

33. Liu, T.; Zhang, B.; Yuan, Y.; Li, M. Real-Time Precise Point Positioning (RTPPP) with raw observations and its application in real-time regional ionospheric VTEC modeling. *J. Geod.* **2018**, *92*, 1267–1283. [CrossRef]

34. Zha, J.; Zhang, B.; Liu, T.; Hou, P. Ionosphere-weighted undifferenced and uncombined PPP-RTK: Theoretical models and experimental results. *GPS Solut.* **2021**, *25*, 135. [CrossRef]

35. Zhang, B.; Chen, Y.; Yuan, Y. PPP-RTK based on undifferenced and uncombined observations: Theoretical and practical aspects. *J. Geod.* **2019**, *93*, 1011–1024. [CrossRef]

36. Zhang, B.; Teunissen, P.J. Characterization of multi-GNSS between-receiver differential code biases using zero and short baselines. *Sci. Bull.* **2015**, *60*, 1840–1849. [CrossRef]

37. Zhang, B.; Teunissen, P.J.; Odijk, D. A novel un-differenced PPP-RTK concept. *J. Navig.* **2011**, *64*, S180–S191. [CrossRef]

38. Guo, F.; Li, X.; Liu, W. Mitigating BeiDou satellite-induced code bias: Taking into account the stochastic model of corrections. *Sensors* **2016**, *16*, 909. [CrossRef]

39. Montenbruck, O.; Schmid, R.; Mercier, F.; Steigenberger, P.; Noll, C.; Fatkulin, R.; Kogure, S.; Ganeshan, A.S. GNSS satellite geometry and attitude models. *Adv. Space Res.* **2015**, *56*, 1015–1029. [CrossRef]

40. Petit, G.; Luzum, B. *IERS Conventions*; Verlag des Bundesamts für Kartographie und Geodäsie: Frankfurt am Main, Germany, 2010; ISBN 3-89888-989-6.

41. Arnold, D.; Meindl, M.; Beutler, G.; Dach, R.; Schaer, S.; Lutz, S.; Prange, L.; Sośnica, K.; Mervart, L.; Jäggi, A. CODE's new solar radiation pressure model for GNSS orbit determination. *J. Geod.* **2015**, *89*, 775–791. [CrossRef]

42. Montenbruck, O.; Steigenberger, P.; Hauschild, A. Multi-GNSS signal-in-space range error assessment—Methodology and results. *Adv. Space Res.* **2018**, *61*, 3020–3038. [CrossRef]

43. Steigenberger, P.; Montenbruck, O. Consistency of MGEX orbit and clock products. *Engineering* **2020**, *6*, 898–903. [CrossRef]

44. Pearlman, M.R.; Degnan, J.J.; Bosworth, J.M. The international laser ranging service. *Adv. Space Res.* **2002**, *30*, 135–143. [CrossRef]

45. CSNO. *Definitions and Descriptions of BDS/GNSS Satellite Parameters for High Precision Applications*; China Satellite Navigation Office: Beijing, China, 2019. Available online: http://www.beidou.gov.cn/yw/gfgg/201911/W020191126317485269344.pdf (accessed on 12 October 2022). (In Chinese)